Modeling of a microsecond pulsed glow discharge: behavior of the argon excited levels and of the sputtered copper atoms and ions

Annemie Bogaerts* and Renaat Gijbels

University of Antwerp, Department of Chemistry, Universiteitsplein 1, B-2610 Wilrijk-Antwerp, Belgium. E-mail: bogaerts@uia.ua.ac.be

A set of models is developed for a microsecond pulsed glow discharge, to describe the behavior of argon excited levels, including the metastables, as well as the cathodic sputtering and the behavior of sputtered copper atoms and ions. These models are coupled to a hybrid Monte Carlo–fluid model for electrons, argon ions and atoms, which was developed previously, to obtain an overall picture of the pulsed glow discharge. Typical results of the present model are the densities of copper atoms and ions, the level populations of argon and copper excited levels, the erosion rate due to cathode sputtering and the contributions due to argon ion, atom and copper ion bombardment, the rates of various collision processes in the plasma, as well as the optical emission intensities. The results are presented as a function of distance from the cathode and as a function of time during and after the pulse.

Introduction

Driven by a growing interest in the analytical community for pulsed glow discharges in recent years (*e.g.*, refs. 1–16), we started developing a model for an analytical microsecond pulsed glow discharge in argon with a copper cathode. In a previous paper,[17] we have presented a hybrid Monte Carlo–fluid model for the electrons, argon ions and fast argon atoms. The only inputs in the model were the cell dimensions, the applied voltage as a function of time, the gas pressure and gas temperature. The last was assumed to vary in time and this time-behavior was more or less used as a fitting parameter in order to calculate the electrical current and power as a function of time, in agreement with experimental data. Other plasma quantities calculated with this model are the electrical potential distribution, the argon ion and electron density profiles, and the rates of argon ionization and ion–electron recombination, as a function of distance from the cathode and as a function of time during and after the pulse. These quantities are important to obtain a better insight into the microsecond pulsed glow discharge, but they are not of direct analytical interest. The hybrid model provides, however, a necessary basis (*e.g.*, the electrical characteristics and the electron behavior) to describe the analytically more important plasma species in the glow discharge, and should always be developed first, before the analytical behavior can be predicted in a self-consistent way.

In the present paper, we continue with the description of the microsecond pulsed glow discharge, but we focus on the behavior of the analytically important plasma species, such as the argon metastable atoms (as well as argon atoms in other excited levels) and the sputtered copper atoms and ions. The models used to describe these species, *i.e.* a combination of collisional–radiative models and Monte Carlo simulations, will be dealt with below.

Description of the models

The models, which will be presented in this paper, are part of a modeling network that we have developed to describe the various plasma species in an argon glow discharge with a copper cathode. An overview of the different species assumed to be present in the plasma, and of the submodels used to describe these species, is presented in Table 1.

The Monte Carlo and fluid models for the electrons, argon ions and fast argon atoms in the μs-pulsed glow discharge are described in ref. 17. The present paper focuses on the behavior of the excited argon atoms, the sputtering process, and the behavior of the sputtered copper atoms and ions.

Collisional–radiative model for the argon atoms in excited levels

A collisional–radiative model consists of a set of balance equations (one for each excited level) with different production and loss terms. The production and loss processes for the excited levels are due to collisions or due to emission of radiation: hence the name of this model. We have considered 65 argon atomic levels. Most of them are "effective levels", *i.e.*, a group of individual levels with similar excitation energy and quantum numbers; but some levels are considered separately, *e.g.*, the four 4s metastable and resonant levels, because they play an important role in the glow discharge.

The production and loss processes taken into account in the balance equations are electron, fast argon ion and atom impact ionization, excitation and de-excitation between the levels, electron–argon ion radiative and three-body recombination, radiative decay between all levels, and Hornbeck–Molnar associative ionization ($Ar^* + Ar^0 \rightarrow Ar_2^+ + e^-$) for the levels with excitation energy above 14.71 eV (*i.e.*, the ionization potential of Ar_2). Moreover, some additional processes are incorporated for the four 4s levels, *i.e.* Penning ionization of the copper atoms, collisions between two argon atoms in a 4s level leading to the ionization of one of the atoms or to associative ionization (*i.e.* the formation of Ar_2^+), two-body and three-body collisions with argon gas atoms, diffusion and subsequent de-excitation at the cell walls, and radiation trapping for the two 4s resonant levels (*i.e.*, re-absorption of the radiation by the ground state argon atoms).

The 65 balance equations are coupled, since the various excited levels affect each other due to the production and loss processes. Hence, the equations are solved simultaneously at each time-step during the entire pulse and afterglow. More information about this model, such as the energy level scheme and the subdivision in various levels, as well as the data (*e.g.*,

Table 1 Species assumed to be present in the plasma, and models used to describe these species

Species	Models
Fast electrons	Monte Carlo model
Slow electrons	Fluid model
Argon ions	Fluid model
Argon ions in cathode dark space (CDS)	Monte Carlo model
Fast argon atoms in CDS	Monte Carlo model
Argon atoms in excited levels	Collisional–radiative model
Sputtering of copper cathode	Empirical formula
Thermalization of sputtered copper atoms	Monte Carlo model
Copper atoms and ions in ground state and excited levels	Collisional–radiative model
Copper ions in CDS	Monte Carlo model

cross sections, transition probabilities) needed to calculate the production and loss processes can be found in ref. 18, where this model was presented in detail for a dc glow discharge.

Calculation of sputtering at the cathode

Sputtering at the copper cathode can be due to the bombardment of argon ions, fast argon atoms created from the argon ions by elastic collisions, and also by copper ions (*i.e.*, so-called "self-sputtering"). To calculate the flux of sputtered copper atoms from the cathode, we need the flux energy distributions of the argon ions, fast argon atoms and copper ions (*i.e.*, the number of ions or atoms bombarding the cathode per unit time, and as a function of energy), which are calculated in Monte Carlo models (see ref. 17 and also below). These flux energy distributions are combined with an empirical formula for the sputtering yield as a function of the bombarding energy (*i.e.*, the number of sputtered atoms per incoming ion or atom) adopted from ref. 19, to obtain the flux of sputtered atoms.

Monte Carlo model for the thermalization of the sputtered copper atoms

When the copper atoms are sputtered from the cathode, they have a typical energy in the order of 5–15 eV. They lose this energy, however, in the first mm from the cathode, due to elastic collisions with the argon gas atoms, until they are thermalized (which means that they reach the temperature of the argon gas). This thermalization process (*i.e.*, the movement of the copper atoms through the argon gas, and the collisions with the argon gas atoms) is described with a Monte Carlo model. This model was presented in detail for a dc discharge in ref. 20, but the principles are the same for the pulsed discharge, except that the criterion for thermalization is now a function of time, because the argon gas temperature varies in time.[17] The result of this model is a so-called thermalization profile, *i.e.*, the number of copper atoms thermalized as a function of distance from the cathode. It should be mentioned that the characteristic time for thermalization[21] is calculated to be of the order of 10^{-7} s for the conditions under study. This is much shorter than the length of one pulse + afterglow (*i.e.*, 0.005 s, at the pulse repetition frequency of 200 Hz; see below), which means that all copper atoms will be thermalized within one pulse + afterglow.

Collisional-radiative model for the copper atoms and ions

Once the copper atoms are thermalized, we assume that their transport becomes diffusion-dominated. Because the thermalization process occurs on a much shorter time-scale than diffusion,[21] the simulation of both processes can be separated in time, and the thermalization profile serves as the initial distribution for the further description of the transport of the copper atoms. It should be mentioned that the above

assumption of diffusion-dominated transport of the copper atoms is probably justified in a narrow region close to the cathode (where the copper atoms have their highest density, see below), but it seems not to be the best representation in the entire glow discharge system. Indeed, it might well be that the copper atoms move in the plasma under the effect of the argon gas flow. We do not yet consider the effect of the gas flow through the system, but we assume that the argon gas is uniformly distributed in the discharge at thermal velocities. Since it appears from experiment that the gas flow can play an important role in the μs-pulsed glow discharge, particularly for mass spectrometry,[22] we plan to incorporate this effect in our future work.

Beside transport in the plasma, the copper atoms can also become excited or ionized. The behavior of the copper atoms and ions, both in the ground state and in various excited levels, is described with a collisional–radiative model. Eight copper atomic levels, seven copper ion (Cu^+) levels, as well as the Cu^{2+} ions, are considered in this model. Again, some of these levels are individual levels, but most of them are a group of levels with similar excitation energy and quantum numbers. Each of these levels is described with a balance equation with different production and loss terms. The processes taken into account in the balance equations are electron and atom impact ionization from all levels, and excitation and de-excitation between all levels, three-body recombination, radiative decay between all levels, Penning ionization by argon metastable atoms, and asymmetric charge transfer with argon ions. Furthermore, transport of the copper atoms occurs by diffusion, whereas the ions move due to diffusion and migration in the electric field. This collisional–radiative model (with identification of the various levels, and the data needed to calculate the production and loss processes) has been described in detail for a dc discharge in ref. 23.

Monte Carlo model for the copper ions in the CDS

Finally, the behavior of the copper ions in the cathode dark space (CDS; this is the region adjacent to the cathode, characterized by a strong electric field) is also described with a Monte Carlo model. This model is similar to the Monte Carlo model for copper ions that we developed for a dc discharge,[24] but the time-dependency has now to be taken into account, because the electric field in the CDS varies as a function of time (see Fig. 2 in ref. 17). The most important output of this model is the flux energy distribution of the copper ions, which is needed to calculate the amount of sputtering (see above).

Coupling of the models

The models described above are coupled to each other due to the interaction processes between the species; e.g. because of the occurrence of Penning ionization, the copper atom density is required as input in the argon collisional–radiative model and the argon metastable atom density is used as input in the copper collisional–radiative model. Moreover, the models presented here are also coupled to the electron and argon ion models of ref. 17, because they need input data from these models, such as the argon ion density, the electron energy distribution function, *etc.* The entire modeling network is solved iteratively until final convergence is reached, which takes several days on a professional workstation.

Results and discussion

The results of the above described models include the densities and level populations of the plasma species, the erosion rate due to cathode sputtering and the contributions of argon ions, fast argon atoms and copper ions to the sputtering process, the occurrence of collision processes in the plasma, such as Penning
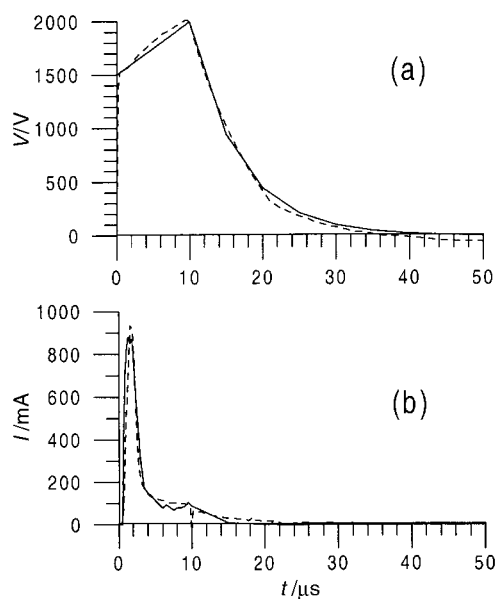
Fig. 1 Applied voltage (a) and resulting electrical current (b) as a function of time during and after the pulse. The solid lines were used as input (for the voltage) and calculated (for the current) in the model,[17] whereas the dashed lines were taken from experiments.[22]

ionization, asymmetric charge transfer and electron impact ionization of sputtered copper atoms, as well as the optical emission intensities of various argon and copper lines. These results will be presented as a function of time during and after the pulse, under the typical experimental conditions used in a microsecond-pulsed Grimm-type glow discharge source,[22] *i.e.*, a 10 μs pulse with a repetition frequency of 200 Hz, an argon gas pressure of 3 Torr, and an applied pulse voltage of about 2 kV.

Fig. 1 shows the applied voltage as well as the resulting electrical current (both calculated in our previous model[17] and measured[22]). The voltage is applied during 10 μs, rising from 1.5 to 2 kV, and drops exponentially to reach more or less zero at about 40 μs. The current is characterized by a distinct peak of almost 900 mA at about 2 μs, and then drops to a plateau value of 100 mA until the end of the pulse (10 μs). After the pulse, it returns to almost zero at about 15–20 μs. The argon ion and electron density follow the same time behavior as the electrical current, as will be illustrated later in this paper [Fig. (5d)]. These results were obtained in our previous paper, but they are repeated here, in order to facilitate comparison with the calculated time behavior of the argon metastable and copper atom and ion densities.

The argon metastable atom density ($4s[3/2]_2$ level) as a function of distance from the cathode is presented at various times during and after the pulse in Fig. 2. The density shows a sharp peak adjacent to the cathode, due to fast argon ion and atom impact excitation, and a broader one due to electron impact excitation. This profile is similar to our results obtained for a dc[18,25] and an rf[26] glow discharge. Fig. 2(a) illustrates that the density rises gradually to a maximum of 10^{14} cm^{-3} near the cathode and *ca.* 4×10^{13} cm^{-3} in the negative glow (NG) at 3 μs, and these values are more or less maintained until the end of the pulse (10 μs), as follows from Fig. 2(b). After 10 μs, the density decreases again, but the decay rate is rather slow, *e.g.*, at 50 μs, the density is still of the order of 5×10^{12} cm^{-3}, which means about one order of magnitude lower than the maximum at 3 μs. This is in contrast to the electrical current and the argon ion and electron densities [see Figs. 1 above and 5(d) below], which become virtually zero at about 20 μs. Hence, it appears that the metastable atoms have a longer lifetime in the afterglow than the argon ions and electrons. This suggests that
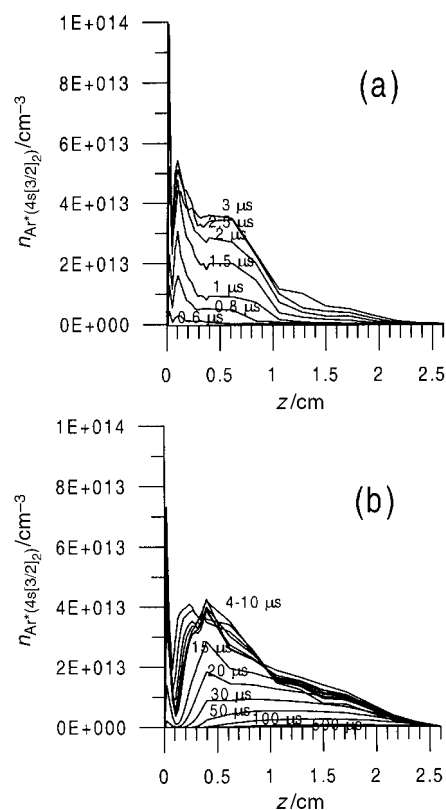

Fig. 2 Calculated argon $4s[3/2]_2$ metastable densities as a function of distance from the cathode, at various times during and after the pulse.

the metastables play a relatively more important role in the afterglow than the argon ions and electrons, which corresponds to statements in the literature (*e.g.*, refs. 1,2). However, at present our calculations cannot yet explain the afterpeak in optical emission and ion intensities of sputtered species, which is observed in millisecond (and sometimes in microsecond) pulsed discharges.[1,2] This afterpeak suggests a change or shift in the ionizing species after discharge termination, and the argon metastable atoms are the most straightforward candidates (*i.e.*, by Penning ionization). Moreover, the measured Ar(I) optical emission intensities appear also to be high in the early afterglow (see below). This suggests that the argon metastable atoms (and the argon excited atoms in general) do not only decay slowly in the afterglow, but they also seem to be created after discharge termination. In the literature it is generally stated that the metastables are formed after the pulse by electron–ion recombination.[1,2] However, using rate coefficients for electron–ion recombination found in the literature (for the values, see ref. 17), our calculations predict that this would not be an important production process of the metastables (see also Figs. 4 and 5 in ref. 17). Hence, it should be concluded at present that either recombination is underestimated in our model (because the rate coefficients from the literature are too low) or that another, yet undefined, production process for the argon metastable atoms needs to be incorporated in the model, which becomes important after discharge termination. In any case, it is suggested that the behavior of the argon metastable atoms in the afterglow is not yet completely correctly described in our model, and that this should be further investigated.

In Fig. 3, the sputtered copper atom density is plotted as a function of distance from the cathode, at different times during and after the pulse. Only the first 4 mm adjacent to the cathode are illustrated, because the density becomes negligible at larger distances. It appears that the density rises rapidly at the beginning of the pulse, until a maximum is again reached at
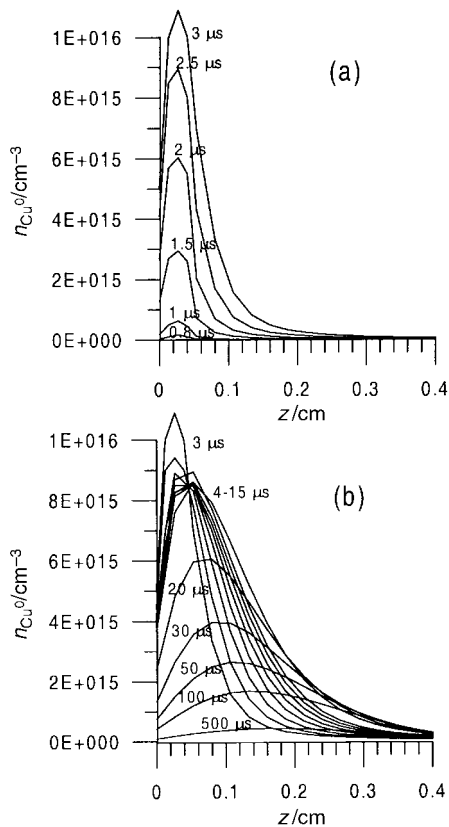
Fig. 3 Calculated copper atom densities as a function of distance from the cathode, at various times during and after the pulse. Only the first 4 mm from the cathode are presented.

Fig. 4 Calculated copper ion densities as a function of distance from the cathode, at various times during and after the pulse. Only the first cm from the cathode is presented.

3 µs. The value at the maximum is in the order of 10^{16} cm^{-3}, which is comparable to the argon gas atom density at 3 Torr. This is quite remarkable, because, in a dc discharge, the sputtered copper atom density was typically calculated to be of the order of 10^{12}–10^{14} cm^{-3}, which is 2–4 orders of magnitude lower than the argon gas atom density.[23,24] However, it should be realized that this maximum value is only characteristic for the very narrow peak adjacent to the cathode (0.2–0.4 mm), and the values in the rest of the discharge are calculated to be much lower (*e.g.*, at $t = 3$ µs: $n_{Cu} = 1.6 \times 10^{15}$ cm^{-3} at $z = 0.1$ cm; $n_{Cu} = 3 \times 10^{14}$ cm^{-3} at $z = 0.2$ cm; $n_{Cu} = 1 \times 10^{14}$ cm^{-3} at $z = 0.3$ cm; $n_{Cu} = 7 \times 10^{13}$ cm^{-3} at $z = 0.4$ cm; $n_{Cu} = 8 \times 10^{12}$ cm^{-3} at $z = 1$ cm; $n_{Cu} = 2 \times 10^{12}$ cm^{-3} at $z = 1.5$ cm; and $n_{Cu} = 6 \times 10^{11}$ cm^{-3} at 2 cm from the cathode). During the remainder of the pulse, and even in the first 5 microseconds of the afterglow (*i.e.*, 15 µs), the copper atom density remains rather constant at 8×10^{15} cm^{-3} between 0.2 and 0.8 mm from the cathode, but the density profile becomes slightly broader. Then the density drops gradually, but the decay rate is again rather slow, or in other words, the lifetime is again rather long, comparable to the behavior of the argon metastable atoms. Indeed, at 500 µs, the density at the maximum is still 4.2×10^{14} cm^{-3}, which is only a factor of 20 lower than the value at the maximum of 3 µs. Moreover, at these longer times in the afterglow, the density profiles have become much broader, *i.e.*, more extended toward longer distances, due to diffusion.

The copper ion density spatial profiles are illustrated at various times during and after the pulse in Fig. 4. For the sake of clarity, only the first cm from the cathode is shown, because the density is negligible further away. It appears that the Cu$^+$ ion density does not reach its maximum at 3 µs, like the copper atoms, but increases further till a maximum value of almost 5×10^{12} cm^{-3} at 10 µs. The position of this maximum value is at about 0.2 cm, which is in the beginning of the NG (see Fig. 2 in ref. 17). Also the argon ion and electron densities were found to reach their maximum at this position (see Fig. 3 in ref. 17),
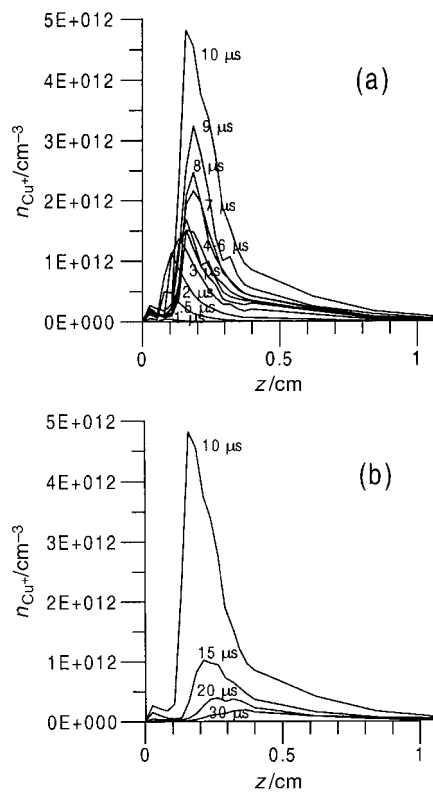
but the maximum was reached between 1.5 and 2 µs. This time-shift in the maximum values of Ar$^+$ and Cu$^+$ ions will be discussed below in more detail (see Fig. 5). After the pulse, the Cu$^+$ ion density appears to drop more rapidly in time than the copper atom density, and it reaches a maximum value of about 2×10^{11} cm^{-3} at 30 µs, which is a factor of 20 lower than the maximum density at 10 µs. The density profiles in the afterglow, however, again become slightly broader, and the position of maximum density is shifted to slightly longer distances from the cathode (*e.g.*, 0.3–0.4 cm at 30 µs).

Fig. 5 presents the calculated densities and level populations of several plasma species, at the maximum of their profile, as a function of time during and after the pulse. As was illustrated before, the argon 4s[3/2]$_2$ metastable level [Fig. 5(a); solid line] shows a maximum at 3 µs. The maximum is about 10^{14} cm^{-3}, which corresponds to the narrow peak adjacent to the cathode (see Fig. 2), created by fast argon ion and atom impact excitation. This narrow peak drops after 3 µs to half its maximum value (*i.e.*, 5×10^{13} cm^{-3}), and this value is maintained until the end of the pulse. Because the maximum of the narrow peak is not really representative for the overall metastable density in the discharge, the dashed line in Fig. 5(a) shows the argon metastable level density at 0.5 cm from the cathode. It appears that this value reaches a broad maximum of almost 4×10^{13} cm^{-3} between 3 and 10 µs, and it drops only very slowly after the pulse (*i.e.*, 10 µs). Moreover, it is clear that the values at the maximum of its profile and at 0.5 cm from the cathode are more or less the same after the pulse, which means that the maximum is now at about 0.5 cm from the cathode [see also Fig. 2(b)]. At 50 µs, the metastable density is still about 5×10^{12} cm^{-3}, *i.e.*, only a factor of 20 lower than the peak value at the maximum, and less than a factor of 10 lower than the maximum value at 0.5 cm. At 100 µs, the density is still 2.6×10^{12} cm^{-3}, and even at 500 µs, it is still 8×10^{11} cm^{-3} at its maximum. Hence, this shows that the argon metastable atoms have a rather long lifetime in the afterglow, at least much
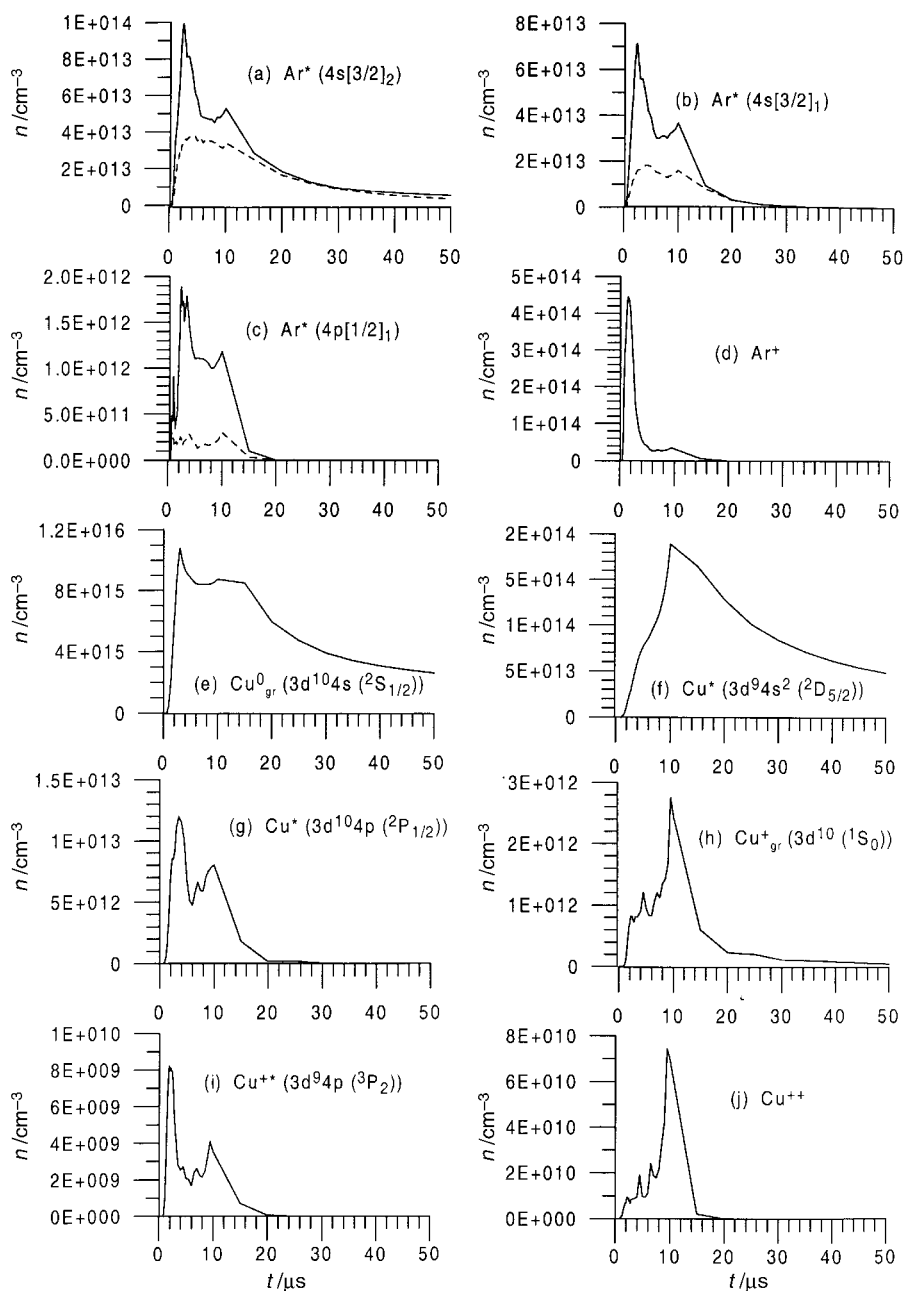
Fig. 5 Calculated densities of various plasma species in ground or excited levels, at the maximum of their profiles, as a function of time. The dashed lines in Fig. 5(a)–(c) represent the densities of the argon excited levels at a distance of 0.5 cm from the cathode.

longer than the argon ions and electrons [see below, Fig. 5(d)]. Therefore, it is indeed expected that the argon metastables are relatively more important than the electrons and argon ions in the afterglow. However, our calculations seem not yet able to predict a peak after discharge termination (*i.e.*, the so-called "afterpeak"), which is expected from the literature.[1,2] This suggests that the production of metastable argon atoms after discharge termination is not yet correctly described, either because electron–ion recombination is currently underestimated or because another important production mechanism (which is maybe not yet known) is not yet taken into account, as was already discussed above.

Fig. 5(b) presents the argon 4s[3/2]₁ level, both at the maximum of its profile (*i.e.*, adjacent to the cathode, solid line) and at 0.5 cm from the cathode (dashed line). This 4s level is not metastable but it is a resonant level, which can decay to the argon ground state by emission of radiation, although a significant fraction of this radiation will be reabsorbed by

ground state atoms. It appears from Fig. 5(b) that this resonant level, at the maximum of its profile (*i.e.*, adjacent to the cathode), reaches also a maximum density at 3–4 µs, after which it drops to about half its value until the end of the pulse. The density value at 0.5 cm from the cathode (dashed line) is again characterized by a broad maximum from 3 to 10 µs. The population density of the resonant 4s[3/2]₁ level is slightly lower than the metastable 4s[3/2]₂ level population, because the resonant level can be more easily depopulated, *i.e.*, by radiative decay. Consequently, the lifetime of the resonant level after the pulse is also shorter than the metastable lifetime. Indeed, it appears from Fig. 5(b) that the resonant level population has dropped to virtually zero at 30 µs.

This trend of a shorter lifetime of the level populations in the afterglow seems to be continued for the higher excited levels, which drop even more rapidly and reach more or less zero at about 20 µs. Indeed, the higher excited levels can more easily be depopulated by radiative decay, without re-absorption of the

radiation. Fig. 5(c) shows the argon 4p[1/2]$_1$ level population as a function of time. It is high during the entire pulse [with a peak between 2 and 4 µs for the maximum of the profile adjacent to the cathode, created by fast argon ion and atom impact excitation (solid line), and more or less constant for the overall density (dashed line)], and drops rather rapidly to low values after the pulse. This time behavior was found to be more or less characteristic for all higher excited argon levels. However, it would be expected from experimental Ar(ı) optical emission intensities that the level populations of the argon excited levels are still high for some time after discharge termination [see also below, Fig. 9(a)]. The fact that our calculations do not predict this behavior suggests again that some production mechanisms of the argon excited levels (i.e., electron–ion recombination or another yet undefined process) is not yet correctly described. This discrepancy needs more investigation in the future.

Fig. 5(d) illustrates the argon ion density, at the maximum of its profile (see Fig. 3 of ref. 17), as a function of time during and after the pulse. The electron density is characterized by exactly the same time profile. The density reaches a distinct maximum of 4.5×10^{14} cm^{-3} at 2 µs, and drops then significantly to a plateau value of about 3×10^{13} cm^{-3} during the rest of the pulse. After 10 µs, the density drops quite rapidly. We calculated a maximum density of 6×10^{12} cm^{-3} at 15 µs, 6×10^{11} cm^{-3} at 20 µs, 1×10^{11} cm^{-3} at 25 µs, 3×10^{10} cm^{-3} at 30 µs, 3×10^{8} cm^{-3} at 40 µs and 8×10^{7} cm^{-3} at 50 µs. This time behavior is very similar to the one for the electrical current, which is logical because the argon ions and electrons determine the current. Since this was found to be in good agreement with the experiment (see Fig. 1), it is expected that the time behavior of the argon ion and electron density is also satisfactorily predicted by our model. When comparing Figs. 5(a) and 5(d), it is apparent that the argon ions and electrons have a higher calculated density than the argon metastables at about 2 µs, but the densities of argon ions and metastables were found to be comparable during the rest of the pulse. In the afterglow, however, the argon metastable density was calculated to be clearly higher than the argon ion and electron densities (see above), which suggests that the argon metastables are indeed more important than the argon ions and electrons during the afterglow.

The density of the copper atoms in the ground state, again at the maximum of its profile, is plotted against time in Fig. 5(e). It reaches a peak of about 10^{16} cm^{-3} (see also Fig. 3) at 3 µs, but it appears to remain high during the entire pulse and even in the first 5 µs after the pulse. After 15 µs, the density decreases, but not very rapidly. Indeed, at 50 µs its maximum value is still 2.6×10^{15} cm^{-3}, at 100 µs it is 1.7×10^{15} cm^{-3}, at 500 µs it is about 5×10^{14} cm^{-3} and at 5000 µs (i.e., the end of the afterglow, or the beginning of the next pulse) we calculated a maximum density of almost 2×10^{13} cm^{-3}. Hence, it appears from our calculations that the sputtered copper atom ground state density has a very long lifetime, because it can only become lost by sticking to the walls, by pumping away, or by electron impact excitation and ionization. However, the latter processes were found to be clearly negligible compared to sticking to the walls, certainly in the afterglow. In our model, the pumping is not incorporated as a loss process. Although we think it is of minor importance compared to the sticking to the walls, the calculated decay rate might be somewhat too low. However, in ref. 27 the lifetime of the copper atom concentration is estimated to be 3–4 ms, which is of the same order of magnitude as our model predictions; hence, it is expected that the general trend of a long lifetime is at least correctly predicted in the model.

The copper atom density presented in Fig. 5(e) corresponds only to the ground state. However, when comparing with Fig. 3, it is clear that this density is practically equal to the total copper atom density, and that the excited levels have a much lower population density. This is illustrated in Fig. 5(f) and (g),

which shows the lowest copper atom excited level (i.e., the metastable 3d^{9}4s^2 ^{2}D$_{5/2}$ level) and the lowest non-metastable level (i.e., 3d^{10}4p ^{2}P$_{1/2}$), respectively. The copper metastable level appears to reach a maximum of almost 2×10^{14} cm^{-3} at the end of the pulse (10 µs) and it decays during the afterglow at a rate that is only slightly higher than the copper atom ground state decay rate. Indeed, the loss processes of the copper atom metastable level are limited to electron impact excitation, de-excitation and ionization (which are expected to be more or less negligible during the afterglow) and de-excitation at the cell walls. The non-metastable copper atom excited levels can, however, more easily be depopulated by radiative decay, and their lifetime in the afterglow is therefore calculated to be much shorter, as appears from Fig. 5(g). This excited copper atom level shows a maximum density at 3–4 µs (i.e., where the copper atom ground state density is at its maximum) and a second, smaller peak at 10 µs. The latter is a bit unexpected, because the most important production process for this copper atom excited level is electron impact excitation from the copper atom ground state,[23] and the electron density reaches a maximum at 2 µs [see Fig. 5(d)]. However, even when the calculated electron density (which refers almost exclusively to the slow electrons) has dropped, electron impact excitation (which is caused by the fast electrons; for the subdivision between fast and slow electrons, see e.g., ref. 17) was calculated to be still rather high at 10 µs. It appears even from the calculations that electron impact excitation and ionization reach a second, minor peak at about 10 µs, as is illustrated for the ionization rate in Fig. 5 of ref. 17. Moreover, at 10 µs, our model predicts that the copper atom ground state density has moved already somewhat further into the discharge by diffusion than at the beginning of the pulse, and it extends somewhat more in the NG, where electron impact excitation is most important. This better overlap between the copper atom ground state density and the region of most efficient electron impact excitation seems to give rise to the second, smaller peak in the copper atom excited level populations at 10 µs. However, it should be mentioned that the measured Cu I optical emission lines show only a maximum at the beginning of the pulse[22] [see also below: Fig. 9(b)]. Hence, this suggests that our calculated level populations of the copper atom excited levels at 10 µs are somewhat too high, and that either electron impact excitation and/or the copper atom ground state density at the end of the pulse are actually overestimated in the model.

The Cu$^+$ ion ground state density at its maximum is plotted against time in Fig. 5(h). It appears to reach its peak value (of about 3×10^{12} cm^{-3}) at 10 µs. The reason for this is probably the same as was calculated for the copper atom excited levels, i.e., at 10 µs the model predicts the best overlap between the copper atom density and the region of most efficient electron impact ionization and, more importantly, Penning ionization. After the pulse, the Cu$^+$ ion ground state density drops rather rapidly to low values, as is illustrated in Fig. 5(h). Hence, the lifetime of the copper ions appears to be much shorter than the copper atom lifetime. This behavior appears to be characteristic for all charged species in the glow discharge (electrons, argon and copper ions), because they can be lost more easily by recombination at the cell walls. Nevertheless, by comparing Fig. 5(d) and (h), it becomes clear that the copper ions reach their maximum much later in the pulse than the argon ions. This is, at least qualitatively, in accordance with time-of-flight mass spectrometry (TOF-MS), which reveals also that the Ar$^+$ ions are created earlier in time than the Cu$^+$ ions. Indeed, the Ar$^+$ ions are typically measured at a delay time between 10 and 50 µs, whereas the Cu$^+$ ions reach their maximum peak at a delay time of about 150 µs.[15] Quantitative comparison for the differences in time between the Ar$^+$ and Cu$^+$ ions can, however, not be made, because our model is limited to the glow discharge behavior, and does not consider the time-of-flight in the mass spectrometer. Indeed, the delay time in TOF-MS is

the time that the ions need to move through the sampler, the skimmer and the ion optics (total length of 14 cm), and it depends on the mass-to-charge ratio of the ions. Therefore, it is more straightforward to compare the calculated ion densities with optical emission signal profiles. The latter show indeed that the Ar II lines have a maximum at the beginning of the pulse (3 μs), whereas the Cu II lines reach a (broad) maximum later in time (5–15 μs); see also below (Fig. 9).

It should be mentioned that the maximum Cu^+ ion ground state density is 2.8×10^{12} cm^{-3}, but a considerable fraction of the copper ions is in the excited metastable levels (see below); hence, the total copper ion density at its maximum is almost 5×10^{12} cm^{-3} (see also Fig. 4). Therefore, by comparing Fig. 5(d) and (h), it appears that the argon ion density at its maximum is about two orders of magnitude higher than the maximum copper ion density. Hence, in the beginning of the pulse, the copper ions are expected to play a negligible role in carrying the electrical current; at about 10 μs, the copper ions contribute for about 10% in the electrical current and their contribution increases further during the afterglow [e.g., at 20 μs, the Cu^+ ion density (ground state + excited levels) is about 4×10^{11} cm^{-3} and the Ar^+ ion density is about 6×10^{11} cm^{-3}; hence the Cu^+ ions are expected to contribute about 40% to the electrical current]. However, the total electrical current during the afterglow is rather low (see Fig. 1), so that the general contribution of Cu^+ ions to the electrical current is expected to be not so important.

As mentioned above, in contrast to the copper atom ground state and excited levels, we found for the Cu^+ ions that a considerable fraction is in excited levels, more specifically in the $3d^9 4s$ metastable levels. The sum of the populations of the four metastable levels is about 2.4×10^{12} cm^{-3} at their maximum, which is almost as high as the Cu^+ ion ground state. Moreover, they are characterized by the same time behavior as the Cu^+ ion ground state. This time behavior is also found for most of the other Cu^+ ion excited levels (which have, however, a much lower population density), but an exception was found for the Cu^+ $3d^9 4p$ $^3P_2$ level, as is illustrated in Fig. 5(i). Indeed, the calculated time behavior of this level population exhibits a major peak at about 2 μs, as well as a minor peak at about 10 μs. The second peak at 10 μs is easily understood, because it corresponds to the maximum in the Cu^+ ion ground state. The first peak arises from the calculated dominant production mechanism of this excited level, i.e., asymmetric charge transfer ionization between argon ions and copper ground state atoms. Since the densities of both species exhibit a maximum at about 2–3 μs, this explains the calculated peak in the Cu^+ $3d^9 4p$ $^3P_2$ level population. However, as will be discussed later, the measured optical emission signal profiles of lines originating from this Cu^+ excited level are not characterized by a peak at 2 μs. This suggests that, for the conditions under investigation, asymmetric charge transfer does not seem to be the dominant production mechanism for the Cu^+ $3d^9 4p$ $^3P_2$ level and, hence, that the level population of the Cu^+ $3d^9 4p$ $^3P_2$ level is not calculated correctly in the model. It should be mentioned that the rate coefficient of asymmetric charge transfer used in the model is subject to large uncertainties. Indeed, because data for asymmetric charge transfer between Ar^+ ions and Cu atoms are not available in the literature, we assumed that the rate coefficient for this process is equal to the Penning ionization rate coefficient (i.e., assumed to be 2.36×10^{-10} cm^3 s^{-1}). This assumption is based on observations in the literature[28,29] for the combinations He–Cd and He–Zn, where the rate coefficients of both processes were found to be comparable to each other if the metal ion possesses suitable energy levels for asymmetric charge transfer (i.e., with a good overlap with the rare gas ion energy levels). Since the Cu^+ ion possesses one energy level that overlaps closely with the argon ion metastable level, we have assumed that the rate coefficient is the same as the one for Penning ionization, but that asymmetric charge

transfer can only occur with the argon metastable ion level (see ref. 23 for more explanation). Moreover, it should be realized that the value we have adopted for the Penning ionization rate coefficient is also subject to some uncertainties, i.e., an experimental or calculated value was also not found in the literature, but we estimated a value based on an empirical formula found in the literature[30] (see again ref. 23 for more details). Hence, due to the uncertainties in the asymmetric charge transfer rate coefficient, it is very probable that this process, and therefore also the population of the Cu^+ $3d^9$ $4p$ $^3P_2$ level, is not calculated correctly in the model.

Finally, Fig. 5(j) illustrates the density of the Cu^{2+} ions at the maximum of their profile, as a function of time during and after the pulse. The Cu^{2+} ion density also appears to reach its maximum at about 10 μs, similar to the Cu^+ ions, but it seems to drop still more rapidly to zero after the pulse.

The flux of sputtered copper atoms, or the sputtering rate, at the cathode is presented as a function of time in Fig. 6, as well as the contributions of fast argon atoms, argon ions and copper ions to the sputtering process. It appears that the sputtering rate reaches a maximum at about 3 μs, which was expected already from the copper atom density behavior, shown in Fig. 5(e). Most of the sputtering during the first 2 μs of the pulse is due to fast argon atoms (ca. 80%), whereas the argon ions contribute to about 20%. This result might seem a bit unexpected, but it was also calculated for dc discharges.[31–33] The reason is that argon ions in the cathode dark space are subject to a large number of elastic collisions with argon gas atoms (i.e., simple scattering collisions and symmetric charge transfer, which is regarded as backward scattering; both are characterized by high cross sections[34]). The energy transfer in these elastic collisions gives rise to "fast" (i.e., non-thermal) argon atoms. The latter can further undergo elastic collisions with argon gas atoms, creating some more fast atoms. This yields a large flux of fast argon atoms bombarding the cathode (see ref. 32). Although the mean energy of these fast argon atoms is a factor of 20 lower than the mean argon ion energy,[32] their flux was found to be almost two orders of magnitude higher,[32] so that they play indeed a dominant role in sputtering.

The copper ions do not yet play a role in sputtering in this initial stage, because there are not enough copper ions formed yet [see Fig. 5(h)]. However, at about 2–3 μs, the contribution of copper ions rises significantly and, at 3 μs, the copper ions and fast argon atoms each contribute about 45% to the sputtering, whereas the argon ions contribute only about 10%. Hence, it appears that, in spite of the lower density and flux of the copper ions compared to the argon ions [see Fig. 5(d) and (h)], their contribution to sputtering is higher, because they are characterized by much higher energies when bombarding the cathode.[23] It should, however, be mentioned that the energy of copper ions bombarding the cathode might be somewhat overestimated in the present calculations. Indeed, in our Monte Carlo model describing the behavior of copper ions in the cathode dark space (see section 2.5), only elastic collisions with argon gas atoms were taken into account and other collision types were neglected. This assumption was certainly justified for the dc discharge (e.g., asymmetric charge transfer with argon gas atoms occurs at a lower rate, and collisions with copper atoms were of lower importance due to the lower copper atom density), and this was also demonstrated by the rather good agreement with experimental copper ion energy distributions.[24] However, as is illustrated in Fig. 3, the copper atom density in the μs-pulsed discharge reaches values only slightly lower than the argon gas atom densities, at least near the cathode, and it is very probable that collisions with copper atoms are not negligible anymore, which might somewhat reduce the copper ion energy at the cathode, and their contribution to sputtering. However, we found that the effect is of minor importance. Indeed, the only effect it has is the creation of some fast copper atoms, which can also contribute
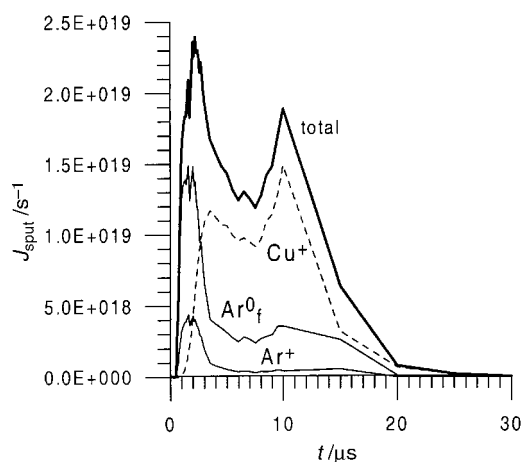
Fig. 6 Calculated sputtering flux at the cathode as a function of time, and contributions of Cu^+ ions, Ar^+ ions and fast argon atoms (Ar^0_f).

to sputtering. Hence, the somewhat lower importance of copper ions to sputtering (due to their slightly lower energy) is compensated by the contribution of fast copper atoms to sputtering, which bombard the cathode at the same time, so that the net effect remains the same.

At later times, the argon ion and fast argon atom fluxes to the cathode drop significantly, in accordance with the drop in electrical current [see Fig. 1(b)] and their relative contribution to the sputtering has decreased to 5% and 20%, respectively. The copper ions, on the other hand, are responsible for as much as 75% of the sputtering during the remainder of the pulse. Indeed, the density and flux of the copper ions rise as a function of time during the pulse, and they reach a maximum at 10 µs. Therefore, the contribution of copper ions to the sputtering is also highest at 10 µs. Hence, this explains the second peak in the sputtering rate at the end of the pulse, which is also sometimes experimentally observed.[22] After 10 µs, the efficiency of copper ions for sputtering also starts to decrease, and the total amount of sputtering drops correspondingly to become negligible at a time of about 30 µs.

In order to calculate the total amount of erosion during one pulse, we do not need the total sputtering flux, but the "net" sputtering flux. Indeed, a significant fraction of the sputtered copper atoms will diffuse back towards the cathode, and will be redeposited. Therefore, we have calculated the net sputtering flux, as the total sputtering flux minus the flux of redepositing copper atoms, and the result is presented in Fig. 7. It appears that the net sputtering flux is not always positive but it can also

take negative values, i.e., at a certain time there can be more redeposition than sputtering of copper atoms. In the first 2–3 µs, the net sputtering flux is highly positive and about 80% of the total sputtering flux. The net sputtering flux, integrated over time (i.e. area 1) amounts to 2.46×10^{13} sputtered atoms. From this, the amount of erosion, in weight loss, can be calculated in eqn. (1) by multiplying by the atomic weight (M in g mol^{-1}) and dividing by Avogadro's number (N_A):

$$ER = \int_{area1} J_{sput,net} dt \frac{M}{N_A}$$

This yielded a net weight loss of 2.6 ng during the time interval corresponding to area 1. From about 2.5 to 9 µs (i.e., area 2) the net sputtering flux was found to be negative (i.e., more redeposition than sputtering). Hence, this yielded a weight gain instead of a weight loss, or a negative amount of erosion of −1.24 ng. From 10 to 15 µs (corresponding to area 3), the net sputtering flux was again positive, yielding a net erosion of 1.15 ng. During the remaining time of the afterglow, the net sputtering flux was found to be slightly negative, which yielded, integrated over time until the beginning of the next pulse, a negative erosion of −1.09 ng. The sum of the net amounts of erosion of parts 1, 2, 3 and 4 gives the total erosion during one pulse. It was calculated to be 1.42 ng. The total erosion per pulse was also measured for the same conditions as used in our calculations, and an experimental value of 1.94 ng per pulse was obtained.[22] Hence, our calculated value is about 25% lower. This reasonable agreement is not so straightforward, because the total erosion in one pulse is the difference of two large numbers (i.e., total sputtering flux minus flux of redepositing atoms), and significant errors can therefore be introduced in the calculations. Hence, the reasonable correlation suggests that our model gives a satisfactory picture of the sputtering process in a microsecond pulsed glow discharge, although complete evidence of the exact sputtering mechanisms cannot yet be given simply by the comparison of these final, time-integrated numbers. This can only be done by more detailed comparison, e.g., of the sputtering rates as a function of time, which we would like to carry out in the future if possible.

Our model is also able to predict the importance of various collision processes in the plasma, as a function of time during and after the pulse. Fig. 8 presents the total amount of ionization of copper atoms as a function of time, as well as the individual contributions of Penning ionization by argon metastables (PI), electron impact ionization (EI) and asymmetric charge transfer with argon ions (CT). It appears that the
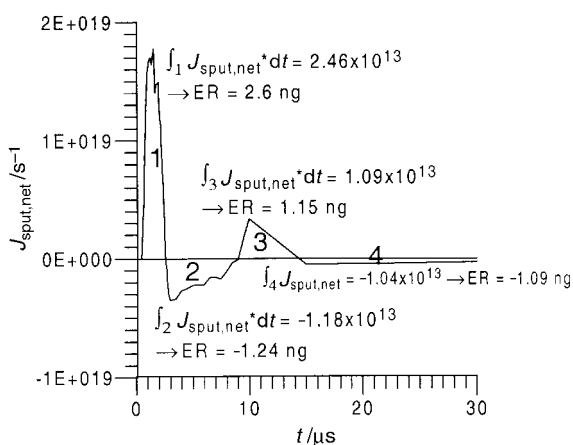

Fig. 7 Calculated net sputtering flux at the cathode as a function of time, and calculated net amounts of erosion (ER) during four time intervals of the pulse.
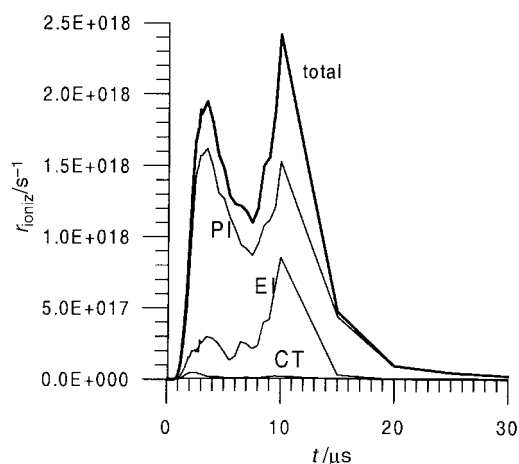

Fig. 8 Calculated ionization rate of copper atoms as a function of time, and contributions of Penning ionization (PI), electron impact ionization (EI) and asymmetric charge transfer (CT).
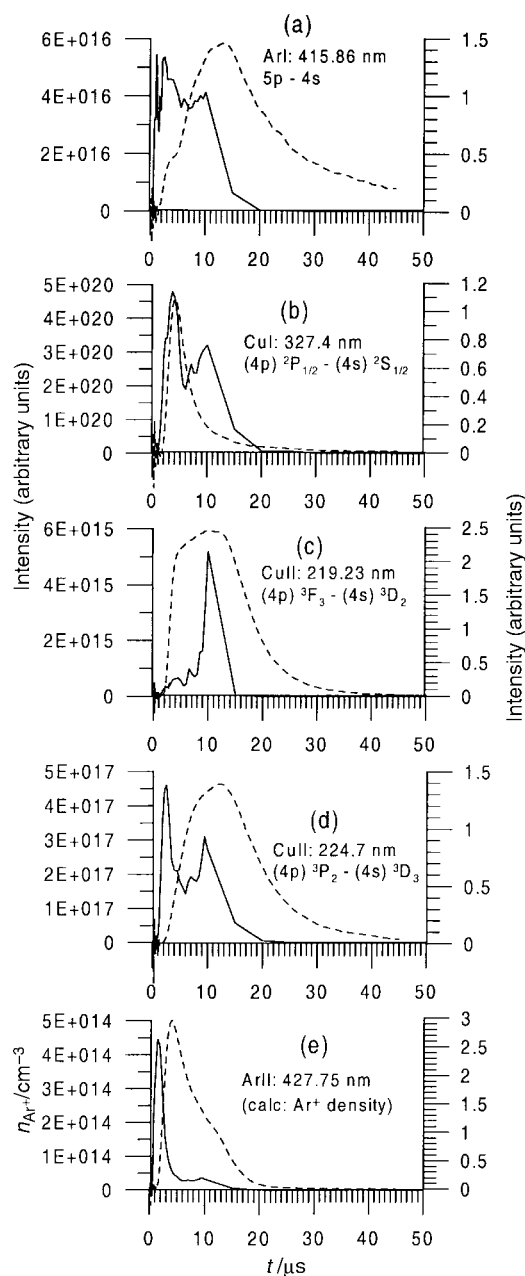
Fig. 9 Calculated (solid lines, left axis) and measured[22] (dashed lines, right axis) optical emission intensities, integrated in the axial direction, as a function of time, of some selected argon and copper atom and ion lines. Fig. 9(e) does not show the calculated Ar II optical emission intensity (which cannot yet be obtained from the model), but the calculated Ar$^+$ ion ground state density.

ionization reaches two maxima, one at about 3 μs and the other at about 10 μs. Further, it is clear that Penning ionization is responsible for most of the ionization of the copper atoms (with a contribution between 70% and 100% during the entire pulse and afterglow), and that this ionization mechanism also reaches two maxima, at about 3 and 10 μs. Indeed, both the argon metastable atoms and the sputtered copper atoms are characterized by their maximum density and by the best overlap in densities at these times, respectively. Electron impact ionization appears to be also quite important, especially at about 10 μs (contribution of 30% at maximum). The reason for this was mentioned before, *i.e.*, at 10 μs, the copper atoms are slightly more extended in the NG by diffusion, where the most efficient electron impact ionization takes place. Asymmetric charge transfer, which was predicted to be the dominant population mechanism for the Cu$^+$ 3d^{9}4p ^{3}P$_2$ excited level

[although from comparison with experimental data, this might be overestimated; see also above, Fig. 5(i)], was found to be of minor importance as a general ionization mechanism for copper with a maximum contribution of less than 10% between 1 and 2 μs, where the argon ions have their maximum density. This finding of the minor role of asymmetric charge transfer is in contrast to our observations for dc Grimm-type discharges, where asymmetric charge transfer could be as important as Penning ionization for the ionization of copper atoms, assuming the same rate coefficient (see the discussion above).[35] The important role of asymmetric charge transfer in dc Grimm-type glow discharges was also demonstrated by the dominant peak of the Cu II 224.7 nm line in the optical emission spectrum.[36] Indeed, this line originates from the Cu$^+$ 3d^{10}4p ^{3}P$_2$ level, which is expected to be populated by asymmetric charge transfer with argon ions (see also above). It is, however, stated in ref. 27 that in a dc discharge, the Cu II 224.7 nm line has a higher optical emission intensity than the Cu I 282.4 nm line, whereas the relative intensities are reversed in a μs-pulsed discharge. This suggests also that asymmetric charge transfer is more important in a dc discharge than in a μs-pulsed discharge. We think that the reason for the minor role of asymmetric charge transfer in a pulsed discharge is because there is no good time-overlap between argon ions and copper atoms. Indeed, the copper atoms reach their maximum density at about 3 μs, where the argon ion density has already dropped to low values. Moreover, it was suggested earlier in this paper that the actual role of asymmetric charge transfer is still overestimated in our model, probably due to a too high rate coefficient (see the discussion above).

Finally, the level populations of the excited argon atom and copper atom and ion levels also allow the calculation of optical emission intensities. Fig. 9 presents the calculated optical emission intensities, integrated in the axial direction to simulate end-on observation, of some selected Ar I, Cu I and Cu II lines, as a function of time during and after the pulse (solid lines, left axis). The measured intensities of these lines, for the same operating conditions,[22] are also plotted in this figure (dashed lines, right axis).

The calculated Ar I 415.86 nm line intensity plotted in Fig. 9(a) exhibits more or less a broad maximum during the entire pulse, with a somewhat higher value at the beginning of the pulse. This calculated time behavior was found to be characteristic for all Ar I lines, and it corresponds to the time behavior of the argon excited levels, as shown in Fig. 5(a)–(c) (at least for the dashed lines, which represent the density at 0.5 cm from the cathode, which is more characteristic for the overall density in the plasma than the narrow peak adjacent to the cathode). It appears, however, that this calculated optical emission time behavior differs drastically from the measured time behavior, *i.e.*, the measured intensity (dashed line, right axis) reaches a maximum later in time (*i.e.*, at the end of the pulse) and drops much more slowly as a function of time after the pulse. This suggests that the argon collisional–radiative model does not yet give a correct description of the behavior of the argon excited levels. This is not completely unexpected, because the model is very complicated and includes a large number of processes, and it is very possible that some rate coefficients of these processes are subject to errors. Alternatively, some processes are maybe not even included in the model, such as a production process for the argon excited levels at the end of the pulse and in the afterglow. This needs certainly further investigation in the future, *e.g.*, electron–ion recombination seems to be the most logical candidate as a production mechanism in the afterglow (see also above and refs. 1, 2), but how can it be sufficiently important when the argon ion and electron densities have dropped already to very low values, and when the rate coefficients described in the literature[17,37–40] are so low?

The calculated time behavior of the Cu I 327.4 nm line

intensity, which is also characteristic for all other Cu I lines that have been calculated in our model, is illustrated in Fig. 9(b) (solid line, left axis). It appears to reach a maximum at about 3–4 µs, and a second, smaller peak at 10 µs, like the Cu* $3d^{10}$ 4p $^2P_{1/2}$ level [see Fig. 5(g)]. The reason for this second peak in the calculation result was given before, *i.e.*, it arises from a better overlap between the copper atom ground state and the region of most efficient electron impact excitation (*i.e.*, beginning of NG) at about 10 µs. However, as is illustrated by the dashed line in Fig. 9(b), the measured line intensity exhibits only a peak at 3–4 µs, and then it drops rapidly. This shows again that our model does not yet give a correct description: it predicts too much electron impact excitation at 10 µs or a too high copper atom density, or too much overlap between both. Again, similar to the argon case, the copper collisional–radiative model is very complicated, and some processes might not be correctly described. Moreover, the fitted gas temperature (see ref. 17) might be subject to some errors, possibly resulting in a too high or too low gas density, and hence in some over- or underestimation of electron impact excitation at a given time (*e.g.*, overestimation at the end of the pulse). Nevertheless, beside the second peak in the calculated intensity at the end of the pulse, the correlation with the experimental time behavior is not too bad.

Fig. 9(c) presents the line intensity of a Cu II line, at 219.23 nm, as a function of time during and after the pulse (solid line, left axis). The intensity is rather low during the entire pulse, but it increases as a function of time, and reaches a pronounced maximum at 10 µs, which corresponds also to the maximum in the Cu$^+$ ion ground state density [see Fig. (5h)]. This calculation result is, however, again not in very good agreement with the measured intensity, which has a much broader maximum, starting earlier in the pulse and extending further in the afterglow (dashed line). This suggests again that some processes are not correctly described or are even not yet incorporated in the collisional–radiative model.

The calculated time behavior of Fig. 9(c) was found to be characteristic for most of the other Cu II lines, but some lines appear to exhibit a different behavior, according to our calculations. Indeed, the lines originating from the Cu$^+$ $3d^9$4p $^3P_2$ level, such as the Cu II 224.7 nm line, appear to be characterized by a dominant peak at 2 µs, beside the peak at 10 µs [see Fig. 9(d)]. The reason was explained above: the Cu$^+$ $3d^9$4p $^3P_2$ level was found to be populated almost exclusively by asymmetric charge transfer ionization of copper ground state atoms with argon ions and, since the latter exhibit a pronounced peak at 2 µs, asymmetric charge transfer was expected to be especially important at about 2 µs. This resulted in the major peak at 2 µs in the time behavior of the Cu$^+$ $3d^9$4p $^3P_2$ level density [Fig. 5(i)] and in the 224.7 nm line intensity [Fig. 9(d)]. However, as shown by the dashed line in Fig. 9(d), this calculated time behavior is again in discrepancy with the experimental data, which are characterized by a broad maximum at the end of the pulse, similar to the Cu II 219.23 nm line intensity. It was, indeed, experimentally observed that all Cu II lines exhibit the same time behavior.[22] This strongly suggests that asymmetric charge transfer is not important in the µs- pulsed discharge for the conditions under study (see also above), and that it is still overestimated in our model (which is not too unexpected, due to the uncertainties in the rate coefficient, see the discussion above).

Finally, Fig. 9(e) presents the measured Ar II 427.75 nm line intensity as a function of time (dashed line, right axis). Since our argon collisional–radiative model does not include argon ionic levels, we are not yet able to calculate Ar II optical emission intensities. However, Fig. 9(e) illustrates, for comparison, the time behavior of the argon ion ground state density (solid line, left axis). It is clear that both the calculated ion density and the measured Ar II emission signal are characterized by a peak in the beginning of the pulse, but again the

measured intensity is broader and drops much more slowly as a function of time than the calculated ion density, and this discrepancy is probably not due to the fact that the calculated result refers only to the density whereas the experimental data are the real optical emission intensities.

In general, it can be concluded that the calculated time behavior of the optical emission signals does not yet fully reflect the real situation. Except for the Cu I emission intensity, the calculated emission signals appear to be characterized by a peak intensity, which is too narrow, or which occurs too early in the pulse, and drops too quickly as a function of time in the afterglow. This suggests that the model cannot yet give a correct picture of the time behavior of excited levels and optical emission intensities. This discrepancy certainly needs further investigation in the near future. Nevertheless, the general trend of the optical emission signals (*i.e.*, the Ar I lines have a broad maximum; the Ar II lines are characterized by a more narrow peak in the beginning of the pulse, as well as the Cu I lines; and the Cu II lines exhibit a broad maximum, rather at the end of the pulse and in the early afterglow) is more or less correctly predicted by the calculations.

Conclusion

A set of models has been developed to calculate the behavior of argon metastable atoms, argon atoms in other excited levels, sputtered copper atoms and ions, both in the ground state and in excited levels, in a µs-pulsed glow discharge. This set of models includes a collisional–radiative model for 64 argon excited levels (with 605 transitions), an empirical formula to calculate the sputtering flux, a Monte Carlo model to simulate the thermalization process of the sputtered copper atoms, a collisional–radiative model for 8 copper atomic and 7 Cu$^+$ ionic levels, as well as for the Cu^{2+} levels (altogether with 103 transitions), and a Monte Carlo model for the copper ions in the cathode dark space.

Typical results of this model, such as the densities and level populations of these plasma species, have been presented as a function of time during and after the pulse. Moreover, the sputtering rate, and the contributions of copper ions (self-sputtering), fast argon atoms and argon ions to the sputtering process have been calculated as a function of time. We found that the fast argon atoms play the most important role for sputtering in the first 1–3 µs of the pulse, whereas the copper ions become dominant after 3 µs. From the net sputtering flux, the erosion rate could be calculated, and the net amount of erosion during one pulse was found to be 1.42 ng. This value corresponded rather well with the experimental value of 1.94 ng, especially when one takes into account that it is calculated as the difference between two large numbers (*i.e.,* the total sputtering flux minus the flux of redepositing copper atoms) and that it is, therefore, subject to considerable calculation errors. The models provide also information about the importance of collision processes in the plasma, as a function of time. It was predicted that Penning ionization is the dominant ionization mechanism of the sputtered copper atoms, followed by electron impact ionization. Asymmetric charge transfer ionization, on the other hand, was found to be of minor importance, probably due to the bad overlap in time of the maximum densities of the argon ions and the sputtered copper atoms. Finally, the calculated time behavior of the optical emission intensities of some selected argon and copper atom and ion lines was presented in this paper, and compared with experimental data. The agreement was not yet satisfactory. This suggests that the model is not yet able to describe the time-dependent behavior of the excited levels and of the optical emission intensities in the correct way. However, to our knowledge, it is the first time that this kind of comprehensive modeling is attempted, and we are aware that there is room for

improvement. In any case, it illustrates also that the μs-pulsed glow discharge is a rather complicated plasma, and that some processes are maybe not yet fully understood. Therefore, the μs-pulsed glow discharge needs certainly more detailed investigation in the near future.

Acknowledgements

References

1 J. A. Klingler, C. M. Barshick and W. W. Harrison, *Anal. Chem.*, 1991, **63**, 2571.
2 F. L. King and C. Pan, *Anal. Chem.*, 1993, **65**, 735.
3 Y. Mei and W. W. Harrison, *Anal. Chem.*, 1996, **68**, 2135.
4 D. C. Duckworth, D. H. Smith and S. A. McLuckey, *J. Anal. At. Spectrom.*, 1997, **12**, 43.
5 R. E. Steiner, C. L. Lewis and F. L. King, *Anal. Chem.*, 1997, **69**, 1715.
6 W. Hang, C. Baker, B. W. Smith, J. D. Winefordner and W. W. Harrison, *J. Anal. At. Spectrom.*, 1997, **12**, 143.
7 W. W. Harrison, W. Hang, X. Yan, K. Ingeneri and C. Shilling, *J. Anal. At. Spectrom.*, 1997, **12**, 891.
8 Y. Su, Z. Zhou, P. Yang, X. Wang and B. Huang, *Spectrochim. Acta, Part B*, 1997, **52**, 633.
9 W. W. Harrison, *J. Anal. At. Spectrom.*, 1998, **13**, 1051.
10 X. Yan, W. Hang, B. W. Smith, J. D. Winefordner and W. W. Harrison, *J. Anal. At. Spectrom.*, 1998, **13**, 1033.
11 C. Yang, K. Ingeneri and W. W. Harrison, *J. Anal. At. Spectrom.*, 1999, **14**, 693.
12 R. E. Steiner, C. L. Lewis and V. Majidi, *J. Anal. At. Spectrom.*, 1999, **14**, 1537.
13 V. Majidi, M. Moser, C. Lewis, W. Hang and F. L. King, *J. Anal. At. Spectrom.*, 2000, **15**, 19.
14 E. Oxley, C. Yang and W. W. Harrison, *J. Anal. At. Spectrom.*, 2000, **15**, 1241.
15 C. Yang, M. Mohill and W. W. Harrison, *J. Anal. At. Spectrom.*, 2000, **15**, 1255.
16 A. Bengtson, C. Yang and W. W. Harrison, *J. Anal. At. Spectrom.*, 2000, **15**, 1279.
17 A. Bogaerts and R. Gijbels, *J. Anal. At. Spectrom.*, 2000, **15**, 895.
18 A. Bogaerts, R. Gijbels and J. Vlcek, *J. Appl. Phys.*, 1998, **84**, 121.
19 N. Matsunami, Y. Yamamura, Y. Itikawa, N. Itoh, Y. Kazumata, S. Miyagawa, K. Morita, R. Shimizu and H. Tawara, *Atom. Data Nucl. Data Tables*, 1984, **31**, 1.
20 A. Bogaerts, M. van Straaten and R. Gijbels, *J. Appl. Phys.*, 1995, **77**, 1868.
21 J. A. Valles-Abarca and A. Gras-Marti, *J. Appl. Phys.*, 1984, **55**, 1370.
22 W. W. Harrison and C. Yang, private communication.
23 A. Bogaerts, R. Gijbels and R. J. Carman, *Spectrochim. Acta, Part B*, 1998, **53**, 1679.
24 A. Bogaerts and R. Gijbels, *J. Appl. Phys.*, 1996, **79**, 1279.
25 A. Bogaerts and R. Gijbels, *Phys. Rev. A*, 1995, **52**, 3743.
26 A. Bogaerts and R. Gijbels, *Spectrochim. Acta, Part B*, 2000, **55**, 263.
27 W. O. Walden, W. Hang, B. W. Smith, J. D. Winefordner and W. W. Harrison, *Fresenius' J. Anal. Chem.*, 1996, **355**, 442.
28 P. Baltayan, J. C. Pebay-Peyroula and N. Sadeghi, *J. Phys. B*, 1985, **18**, 3618.
29 P. Baltayan, J. C. Pebay-Peyroula and N. Sadeghi, *J. Phys. B*, 1986, **19**, 2695.
30 L. A. Riseberg, W. F. Parks and L. D. Schearer, *Phys. Rev. A*, 1973, **8**, 1962.
31 R. S. Mason and R. M. Allott, *J. Phys. D*, 1994, **27**, 2372.
32 A. Bogaerts, M. van Straaten and R. Gijbels, *Spectrochim. Acta, Part B*, 1995, **50**, 179.
33 I. Revel, L. C. Pitchford and J. P. Boeuf, *J. Appl. Phys.*, 2000, **88**, 2234.
34 A. V. Phelps, *J. Appl. Phys.*, 1994, **76**, 747.
35 A. Bogaerts and R. Gijbels, *Spectrochim. Acta, Part B*, 1998, **53**, 437.
36 E. B. M. Steers and R.J. Fielding, *J. Anal. At. Spectrom.*, 1987, **2**, 239.
37 R. van de Sanden, Ph.D. Thesis, Eindhoven University of Technology, 1991.
38 V. S. Vorob'ev, *Plasma Sources Sci. Technol.*, 1995, **4**, 163.
39 H. S. W. Massey and E. H. S. Burhop, *Electronic and Ion Impact Phenomena*, Oxford University Press, Oxford, 1952.
40 M. A. Biondi, *Phys. Rev.*, 1963, **129**, 1181.